



Ultimate slope design in open pit phosphate mine using geological and geomechanical analysis: case study of Jebel Jebbeus

Rahma Ahmadi¹ · Moufida El May¹ · Mahmoud Dlala¹

Received: 30 September 2018 / Accepted: 6 February 2019 / Published online: 18 April 2019
© Saudi Society for Geosciences 2019

Abstract

Open pit mining of the phosphate deposit in the Meknassy Basin, particularly in Jebel Jebbeus, requires slope design and stability analysis to maintain security and profitability. These processes depend on the geological and geomechanical characteristics of the open pit mine area. Therefore, to identify these characteristics, several studies (geological, structural, geotechnical) were carried out using field surveys and laboratory tests. Two ultimate slope designs were developed based on the characteristics of the geological materials in the area. One slope cut will be performed in the marl, and another will be made in the rock mass. The application of kinematic methods identified two potential failure modes in the rock slope: planar and wedge failures. The maximum slope safety angle in the carbonates is 70°. The stability analysis using the limit equilibrium method indicates that the 42-m-high slope in the marl is stable with a 25° slope angle and that the 70-m high slope in the rock mass is stable with a 70° slope angle.

Keywords Open pit mine · Phosphate deposit · Geological and geomechanical characteristics · Ultimate slope design · Slope stability

Introduction

Mining is a crucial part of the economy in several countries around the world. However, this work sector is unsafe. Mines are mainly exposed to instability risks. The stability of mines and the safety of employees must be a primary objective in any mining operation to ensure the continuity of production and to protect human lives and equipment.

Mining activities in an open pit mine lead to the formation of slopes, which are regarded as geotechnical structures. During the planning process, this type of structure requires dimensioning to ensure both the economic viability and safety of the open pit mine during exploitation by following a basic rule of maximizing the slope angle. The slope geometry is closely linked to the profitability of the mine. The lower the slope inclination is, the lower the production costs are;

however, an overly steep slope can cause instability at the slope edge, which is reflected in a variety of surface displacements that may occur.

Slope stability analysis and design in open pit mines require access to detailed geological, structural, hydrogeological, and geomechanical data. The collection of these data is a continuous process through the life of a mine, from exploration to mine closure.

This paper discusses the geological and geomechanical studies performed to design ultimate slopes in an open pit phosphate mine during the preliminary stage of exploitation. This mine will be excavated in Meknassy Basin (Central Tunisia), where exploration data collected from Jebel Jebbeus revealed a potential phosphate deposit that can be extracted using the open pit mining method.

Editorial handling: Murat Karakus

✉ Moufida El May
elmaymoufida@yahoo.fr

¹ University of Tunis El Manar, Faculty of Sciences of Tunis, UR13ES26, 2092 Tunis, Tunisia

Methodology

The objective of this study is to identify the geometries of stable excavated slopes in an open pit phosphate mine. Thus, we need to follow a well-defined working methodology that includes the studies and methods required to

obtain the ultimate slope design. This process can be divided into two phases.

Phase one includes a detailed study of the field characteristics of the area of the phosphate deposit. This study involves the acquisition of geological and geomechanical data by field observations and measurements and laboratory tests as well as the analysis of the data, which allows the petrographic characteristics of the material (rock or soil), its state of fracturing, and its mechanical properties to be determined (Cojean and Fleurisson 2005; Fleurisson 2012). The analysis of the discontinuity network measurements from the rock mass is based on stereographic projections to identify the geometric parameters of each major discontinuity family (Jhanwar and Barsagade 2010).

Phase two focuses on the slope design by determining the geometric parameters of the ultimate slopes and performing stability analyses, including both kinematic and limit equilibrium stability analyses, for the slope design. The first step in this analysis is to identify the potential modes of deformation and failure (planar, wedge, toppling, and circular failures) that can affect the slope after excavation using kinematic methods based on stereographic projections (Singh et al. 1994). This method identifies the maximum safety

angle, which is one of the slope's geometric parameters. The stability calculation software "Slide" is then used to calculate the safety factor of the designed slope based on the limit equilibrium method.

Geological study

Geographical setting

The study area is located in the southeastern part of central Tunisia. It is located 13 km north of the town of Meknassy and 2 km east of the Meknassy-Sidi Bouzid road (Fig. 1).

Geological setting

The Jebel Meheri-Jebbeus is located along a north-south axis that represents the southern plunge at the northern end of the Meknassy-Mezzouna range. This chain is aligned with a NW-SE-oriented tectonic corridor marked by Triassic outcrops. These outcrops border both flanks of Jebbeus Jebel but do not reach its S-SW part (Jaouadi 1996).

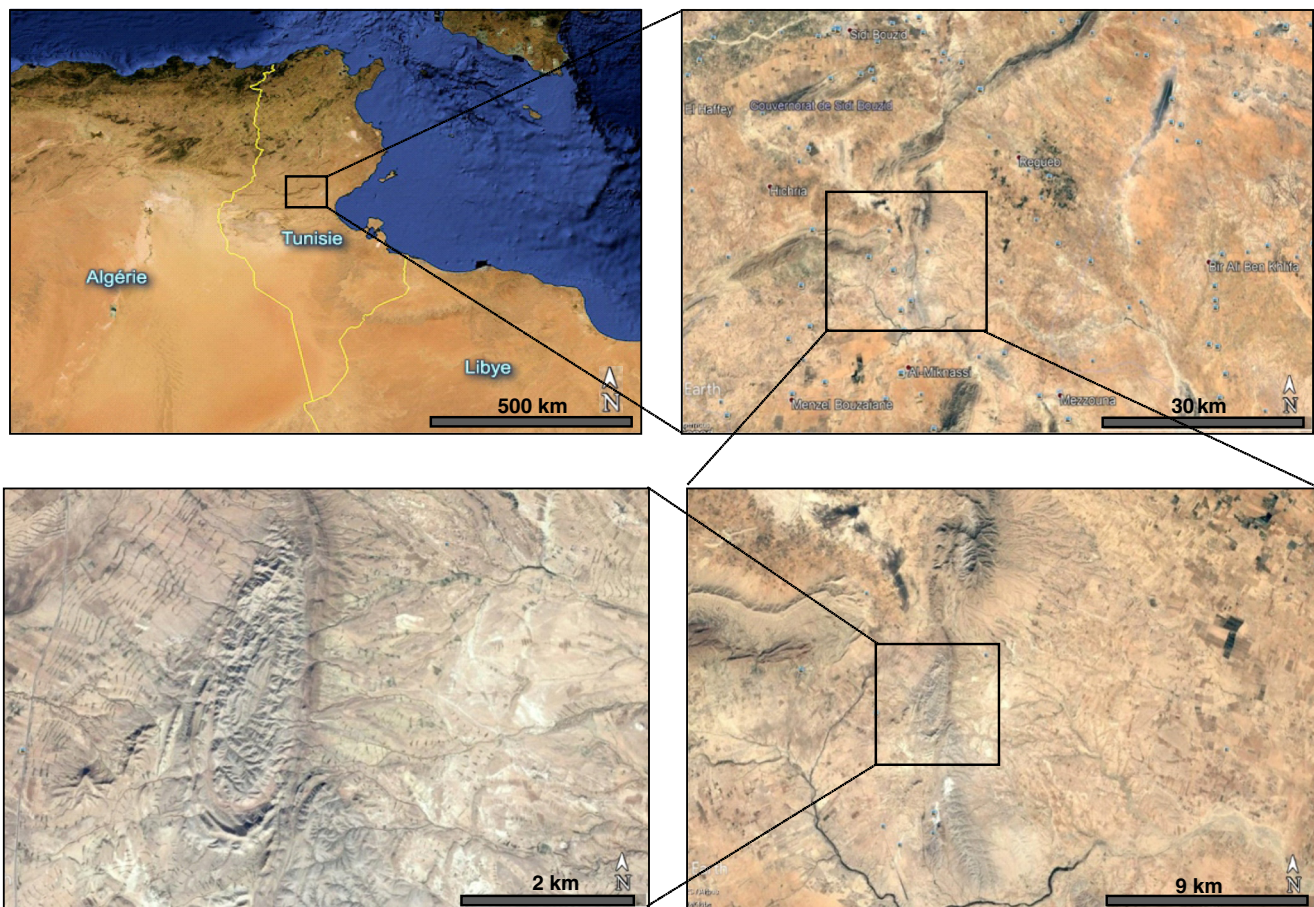


Fig. 1 Location of Jebel Jabbeus, Tunisia in satellite photos

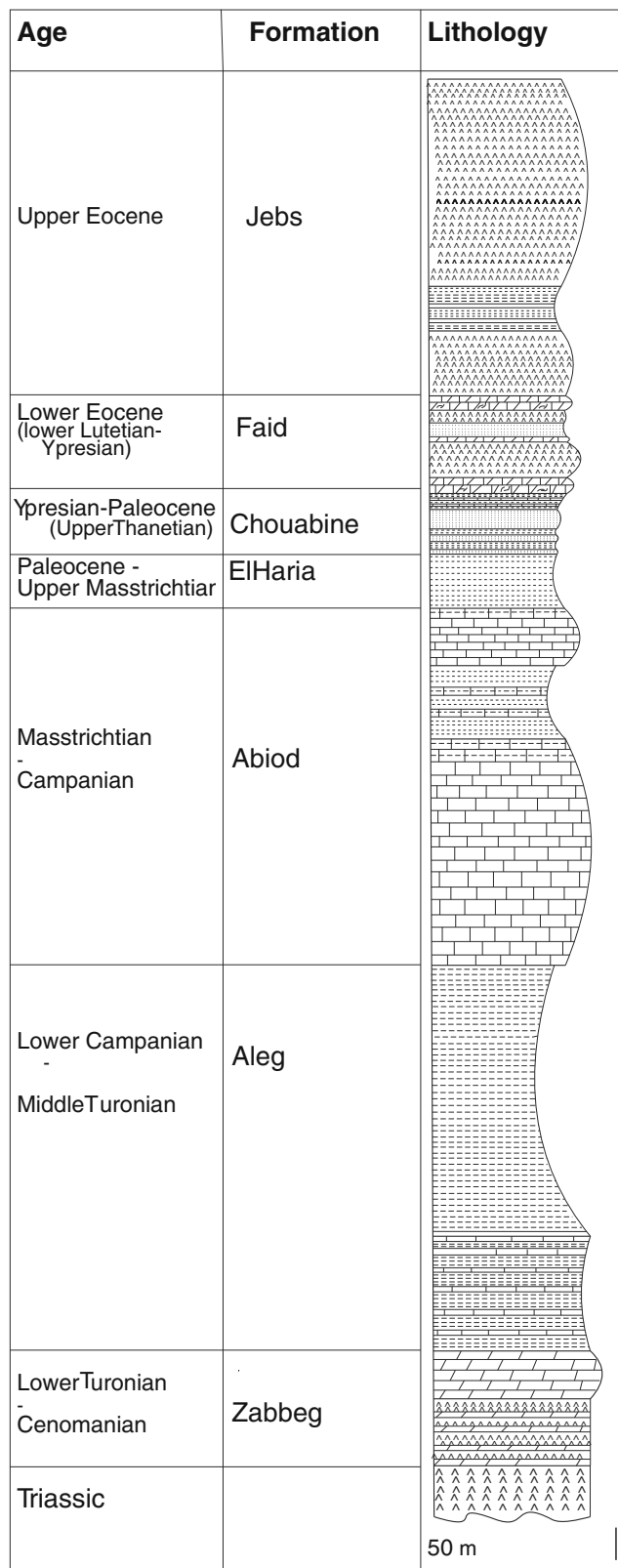


Fig. 3 Synthetic lithostratigraphic column of the Triassic to Upper Eocene deposits at Jbel Jebbeus

- Faïd Formation: The base and the top of this formation are characterized by two dolomitic and lumachelic

intervals with traces of bioturbation at their bases. A massive gypsum layer with a maximum thickness exceeding 100 m is located between the top and base; it contains several layers of dolomite, limestone with sandstone, and a phosphate layer.

- Jebbs Formation: The study area is the type locale of this formation, where it occupies the core of Jebel Meheri Jebbeus (Jaouadi 2004). It has a maximum thickness of 900 m and is divided into three units:
 - The lower unit, which has an average thickness of approximately 40 m, contains white gypsum and anhydrite with thin interlayers of clay and marl.
 - The middle unit consists of a thick layer of reddish clay and thin gypsum deposits. This unit forms a topographically unique reddish valley called the “wine bed.”
 - The upper unit contains a massive layer of whitish to grayish gypsum, thin interlayers of varicolored clays (greenish to grayish and yellowish), and meter-scale dolomitic beds. This unit is approximately 270-m thick.

Structural study

The study area has been affected by significant events that controlled the sedimentation from the Upper Cretaceous to the Eocene and contributed to the evolution of the Jebbeus syncline (Jaouadi 2004). This syncline is bordered by two major faults that intersect at its northern end and give it the shape of a drop: a north-south striking strike-slip fault on the eastern flank and a NE-SW-striking thrust fault on the western flank. Triassic outcrops mark these two faults (Fig. 4).

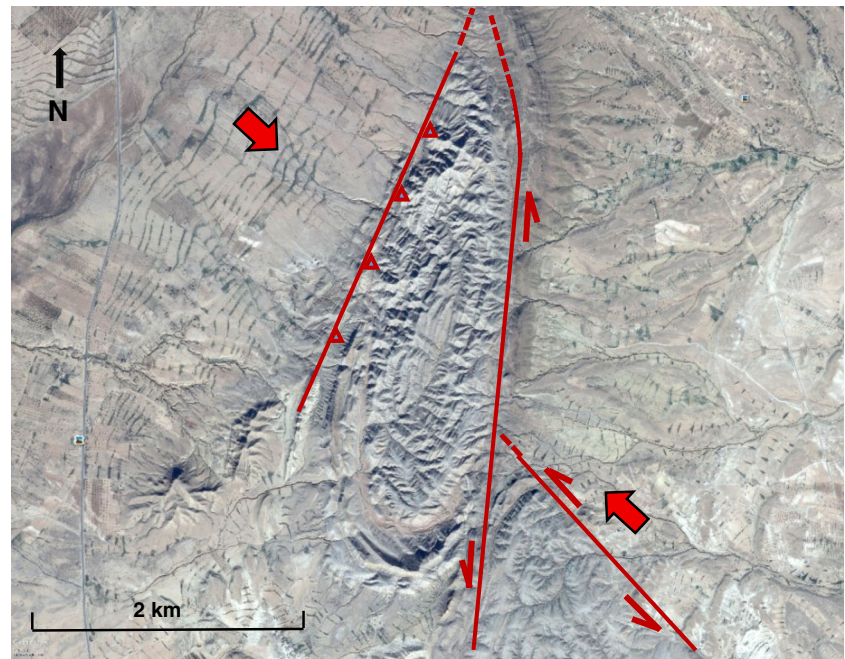
The Jabbeus structure is interpreted as a Paleocene-Eocene unit above the Triassic units (Jaouadi 2004).

The deposits in the study area, which range in age from Upper Cretaceous to Eocene, show significant variations in thickness, including significant thickening at the S-SW closure of the Jabbeus syncline. This thickening consists of a progressive beveling to the north along the Triassic outcrops, where the layers are vertical. This reflects the intensity of shearing in this area and the instability of the sedimentary units, since the Upper Cretaceous is related to halokinetic movements.

These movements were activated by an extensional regime during the deposition of the Aleg Formation that continued during the sedimentation of the Abiod Formation. The deposits of this formation were affected by compressive deformation with a N-NE shortening axis.

As a result of this halokinetic activity, low zones (Rym syncline) formed around the Triassic outcrops. During the Eocene, simultaneous NW-SE and N-S deformation in a compressive regime with a NW-SE shortening direction caused

Fig. 4 Major faults surrounding the El Meheri Jebbeus structure: a north-south striking faults and a northwest-southeast striking fault are located to the east; and a northeast-southwest striking fault bounds the structure to the west



the reactivation of the sinistral subsidiary faults, which caused the thickening of the Jebbs Formation (Jaouadi 2004).

The deformation of the various Jbel Jabbeus deposits, which is mainly due to halokinetic activity, is expressed by several faults that affect these deposits.

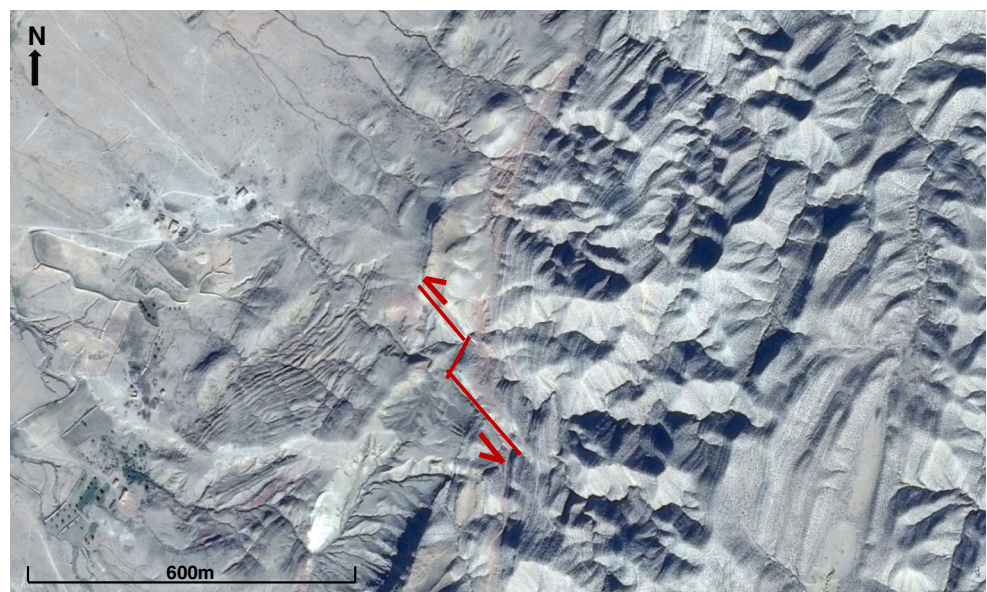
These faults, which are observed throughout the Jabbeus structure, are classified into systems according to their orientations: northwest-southeast (NW-SE), north-south (N-S), northeast-southwest (NE-SW), and east-west (E-W).

- The NE-SW fault system is mainly located at the southwestern closure of the syncline and is composed of

synsedimentary normal faults with lengths of several tens of meters, which affect the lower Eocene deposits. These faults show strike-slip movements that cause local thickening of the affected layers.

- The N-S fault system mainly includes a major fault marked by the Triassic outcrops on the eastern side of the syncline. This is an old sinistral strike-slip fault that is considered to be a part of the N-S axis.
- The NW-SE fault system is considered the most dominant system in the study area, and it includes the major KBR (Khalifa ben Romdhane) Fault. This system is represented by normal faults that are several tens of meters long and

Fig. 5 NW-SE Striking strike-slip fault in the northwestern part of the Jebbeus syncline



particularly affect the upper unit of the Jebbs Formation. One of the major faults in this system is a sinistral strike-slip fault that affects the Paleocene to upper Eocene units as well as the Triassic units in the NW part of Jebel Jabbeus. This fault's orientation is the result of a compressive phase with a NW-SE shortening axis. This fault bounds the phosphate deposit (Fig. 5).

- The E-W fault system contains few faults, which are mainly located on the southwestern side of the study area. A fault of this system affects the Abiod Formation at Jebel Bou Nakta.

Based on these geological and structural studies of Jebel Jabbeus, a geological map was developed. The map shows the limits of the various deposits and the faults that affect them (Fig. 6).

Hydrogeological study

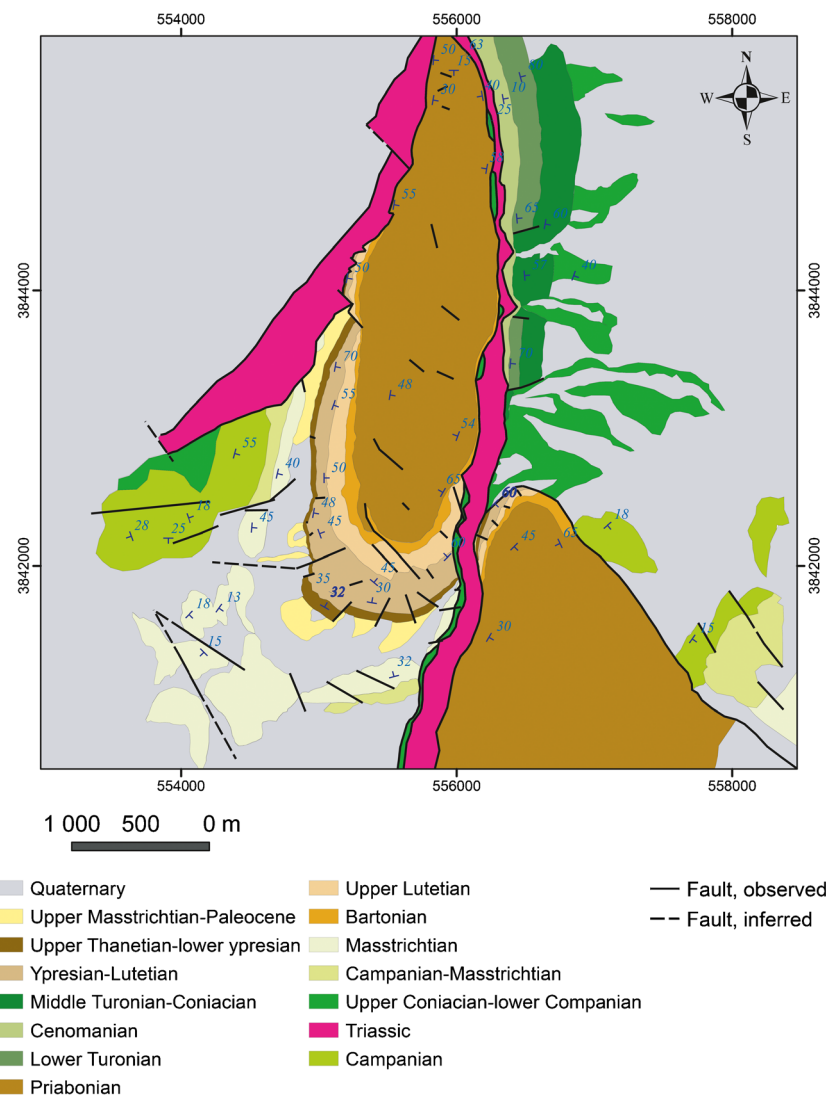
The piezometers placed in the area of the open pit mine show no groundwater to depths of up to 100 m. Therefore, the hydrogeologic conditions do not represent a risk to slope stability.

Phosphate deposit of Jebel Jabbeus

General presentation

The Meheri-Jebbeus Jebel phosphate deposit is limited to the southern and western flanks of the structure over a length of approximately 3200 m. It is not exposed on the eastern and northwestern flanks, where the Triassic units outcrop.

Fig. 6 Geological map of Jebel El Meheri Jabbeus



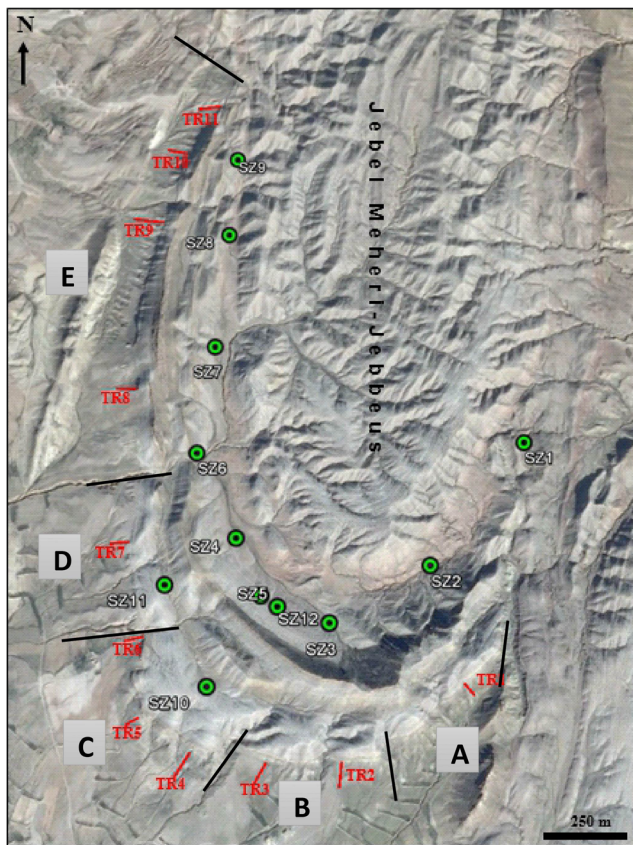


Fig. 7 Locations of sections, trenches, and reconnaissance boreholes in the Jebbeus syncline

However, a smaller phosphate deposit is located on the eastern flank at the northern extremity of Jebel Abdallah. Based on an old exploration study carried out in this area by the “CPG” company, the deposit is divided into five sections bounded by faults with large displacements (from 10 to 30 m). These sections, which are labeled from A to E, are located around the margin of the structure from SE to NW. Sections A, B, and C

cover the southern closure of the structure, whereas sections D and E are located along its western flank (Fig. 7).

The deposit contains two phosphate levels, called the upper and lower, which are separated by a massive gypsum layer with variable thickness (Lafi et al. 2016):

- The upper phosphate level, or “roof phosphate,” which is part of the Faïd Formation, has a maximum thickness of 40 m. It is composed of hard siliceous phosphate with yellowish marl and marly limestone interlayers. This phosphate is very low in P₂O₅, with contents that vary from 7 to 12% (Beji-Sassi 1985). This level could be exploited and enriched by flotation.
- The lower level, which has a variable thickness, generally comprises three phosphate layers (I, II, and III) divided by two marly levels (m1-2 and m2-3). The P₂O₅ contents vary from 24.65 to 26.56% (Beji-Sassi 1985). This phosphate level of the Chouabine Formation has a good ore quality with a high P₂O₅ content, which increases the commercial and economic value of this deposit and particularly of this level.

The lower phosphate level represents the main deposit to be exploited. The upper level is a secondary, non-priority target. This delimits the area to be mined. Therefore, our study focuses specifically on the zone in which the main phosphate level is located.

The thickness of the Metlaoui Group, particularly the Chouabine Formation, where the main phosphate deposit is located, is variable along its outcrop. The maximum thickness is located at the S-SW closure of the syncline. The units decrease in thickness, and some layers even disappear, near the Triassic outcrops on the western flank.

At a more detailed scale, the variation in thickness of the Chouabine Formation is expressed well in the phosphate level, where the three phosphate layers show significant variations in outcrop and depth. Thickness measurements of these layers were taken from a series of trenches and geological reconnaissance drilling in sections A, B, C, D, and E by the Gafsa Phosphates Company as part of its exploration work. These measurements are shown in Tables 1 and 2.

Table 1 Thicknesses (in meters) of phosphate layers and marl interlayers in the trenches (TR)

Sections	A		B			C		D		E		
Layers	TR1	TR2	TR3	TR4	TR5	TR6	TR7	TR8	TR9	TR10	TR11	
CI	2.37	1.6	8.16	15.24	22.37	4.24	9.36	9.7	4.79	–	4.35	
m ₁₋₂	2.62	3.57	8.32	8.5	–	–	2.21	0.18	2.58	2.61	2.49	
CII	0.41	0.44	0.62	0.64	–	–	1.07	0.36	2.57	2.07	1.06	
m ₂₋₃	4.01	7.13	10.33	–	–	2.78	10.71	3.17	4.02	1.15	2.54	
CII	4.01	1.69	6.06	–	–	2.48	0.26	0.72	3.14	1.37	3.33	
CI + CII + C	6.79	3.73	14.84	15.88	21.37	6.78	10.69	10.78	10.5	3.44	8.74	

Table 2 Thicknesses (in meters) of phosphate layers and marly interlayers in the core boreholes (SZ)

Layers	SZ2	SZ3	SZ4	SZ5	SZ6	SZ7	SZ8	SZ9	SZ10	SZ11	SZ12
Depth of CI	231.3	188.8	186.0	185.8	111.5	181.2	212	254	74.8	90.3	183.7
CI	0.24	3.55	4.97	3.54	9.98	10.16	6.38	6.98	13.87	5.43	7.97
m ₁₋₂	2.08	3.20	2.33	–	–	5.44	5.75	4.39	6.53	5.43	4.24
CII	0.16	0.69	0.63	–	–	0.82	2.07	1.08	1.22	0.23	0.85
m ₂₋₃	1.52	5.63	3.12	–	–	5.44	6.20	3.85	6.62	1.55	4.92
CIII	0.48	3.98	2.61	–	–	5.35	5.48	3.31	6.39	3.51	4.32
CI + CII + CIII	0.88	8.23	821	3.55	9.98	16.40	13.93	11.37	21.48	9.17	13.14

Based on the thickness measurements of the phosphate layers in outcrop (Table 1), the maximum thicknesses are located in sections B and C. Table 2 also shows that the thickest phosphate layers are at the shallowest depth in borehole SZ10, which is located in section C. Therefore, the most profitable exploitation of the phosphate layers is in sections B and C, which cover the southern closure of the Jebbeus syncline. Therefore, the fracture study was limited to that area, which was intended to be mined.

The measurements shown in Table 2 indicate that the variation in layer thicknesses at depth and the disappearance of

some layers may be caused by internal faults that affect the deep deposits.

Fracture analysis of the S-SW closure of the Jebbeus structure

The fractures observed in the study area include two types: faults and joints. The thickening of the deposits in the southern closure of the syncline is controlled by a sequence of synsedimentary faults that primarily strike NE-SW. These are

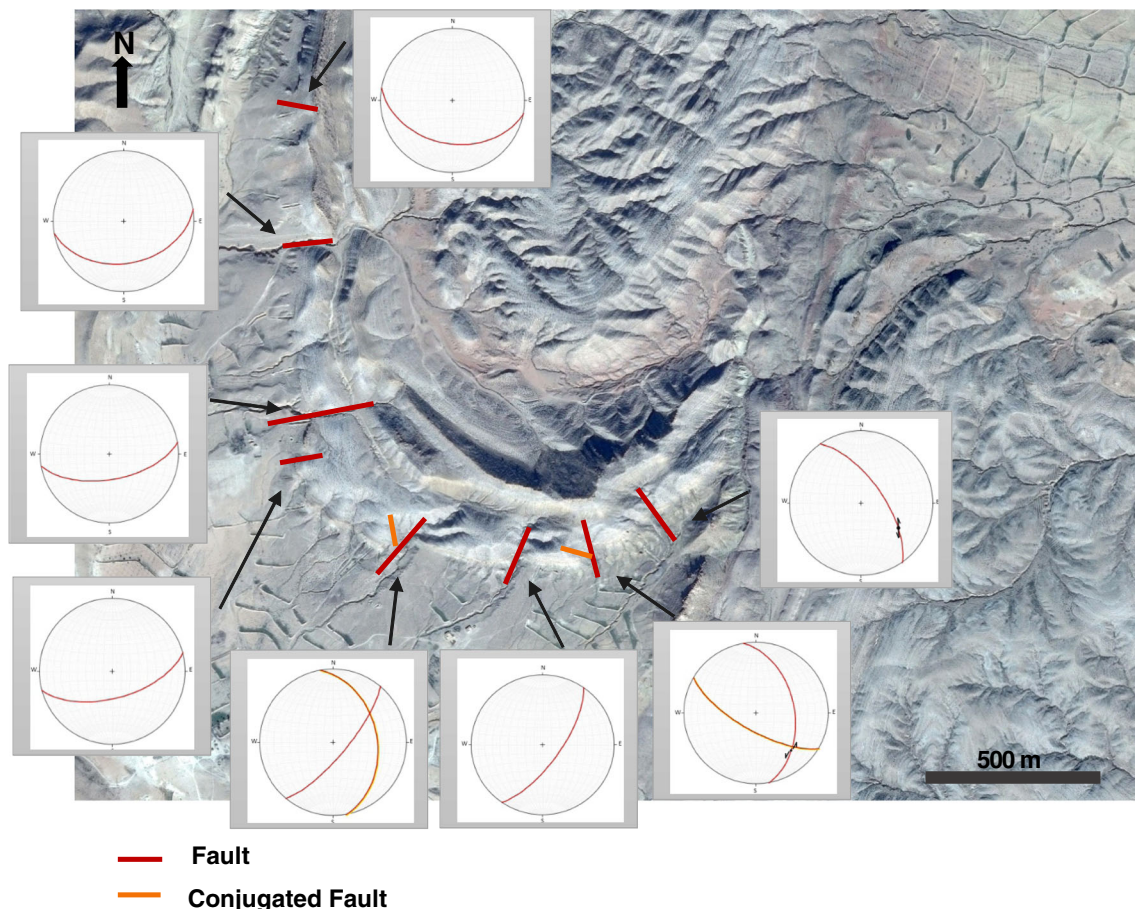


Fig. 8 Stereographic projections of faults on the southern closure of the Jebbeus syncline

normal faults with strike-slip displacements that were activated in an extensional system during the lower Eocene and probably slightly earlier (Paleocene) (Jaouadi 1996; Jaouadi 2004). Based on field observations, several fault characteristics (e.g., strike, dip, rake) are determined and presented in stereographic projections (Wulff nets). These faults, which have displacements varying from 10 to 30 m, are sometimes associated with conjugate faults (Fig. 8).

The presence of carbonate deposits allows the formation of joints induced by these faults and the major faults. This deposit is represented by a fractured dolomitic layer that forms the base of the Faid Formation (lower Eocene) and overlies the main phosphate deposit (Fig. 9). In the southern synclinal closure, this layer is between 5- and 12-m thick. The fracturing of this carbonate layer is one of the main parameters involved in the selection of the phosphate mining methods in sections B and C. According to field observations, the fracture systems differ between the two sections. To understand the geomechanical context and stability of this carbonate layer, a fracture analysis is performed in each section.



a Carbonate deposit fracturing in section B.



b Carbonate deposit fracturing in section C.

Fig. 9 Fracturing of the carbonate layer in sections B and C

Each fracture or joint is characterized by several parameters that are measured in the field along measurement lines covering as much of the study area as possible to obtain a good representation of the fractures affecting the carbonate layer. The fracturing parameters recorded include the orientation (azimuth and dip), continuity or extent, spacing (between fractures of the same family), opening (distance between the fracture walls), filling of openings, moisture and water conditions, and average block size, which is the dimensions of the blocks that the fracture forms (Ruhland et al. 1990; Chalhoub 2006; Tahiri 1992; Porokhovoï 1995).

This method of systematic fracture surveys allows the discontinuity measurements to be classified into families based on orientation using a specific technique (graphs and statistics) and the geometric parameters of each family, such as frequency, density, extent, and spacing, to be determined (Carreon-Freyre et al. 1996).

In section B, 117 fractures were measured over a distance of 350 m. In section C, 131 fracture measurements were collected over a distance of 300 m.

Rose diagrams and stereographic projections

The statistical treatment is applied by drawing a rose diagram of the orientations of the fractures that affect the carbonate layer in the two sections on a semicircular grid divided into classes. The radial axis corresponds to the number of fractures in each class. Preferential directions, indicated by large numbers of discontinuities in a class, represent the main fracture families (Fig. 10a).

The most commonly used graphical processing method is a stereographic projection of discontinuities, which provides a graphical presentation (stereogram) of the fracture strikes and dips on a graduated scale (Wulff net) (Ruhland et al. 1990). Then, based on the two main geometric parameters (orientation and dip), a discontinuity (fracture) classification can be made. The standard deviations of these two parameters provide an estimate of the quality of the choice of the families (Fig. 10b).

The rose diagrams and stereograms shown in Fig. 10 indicate the major fracture families in each section, which are described in Table 3.

Geometric parameters of the major fracture systems

Fracture density

Several fracture parameters are involved in the calculation of the fracture density, which is defined as the sum of the frequencies of the major fracture families:

$$\text{Cumulative frequency} = \text{Density} = \sum \text{Frequencies.}$$

Fig. 10 Stereographic projections and rose diagrams of the fracture measurements

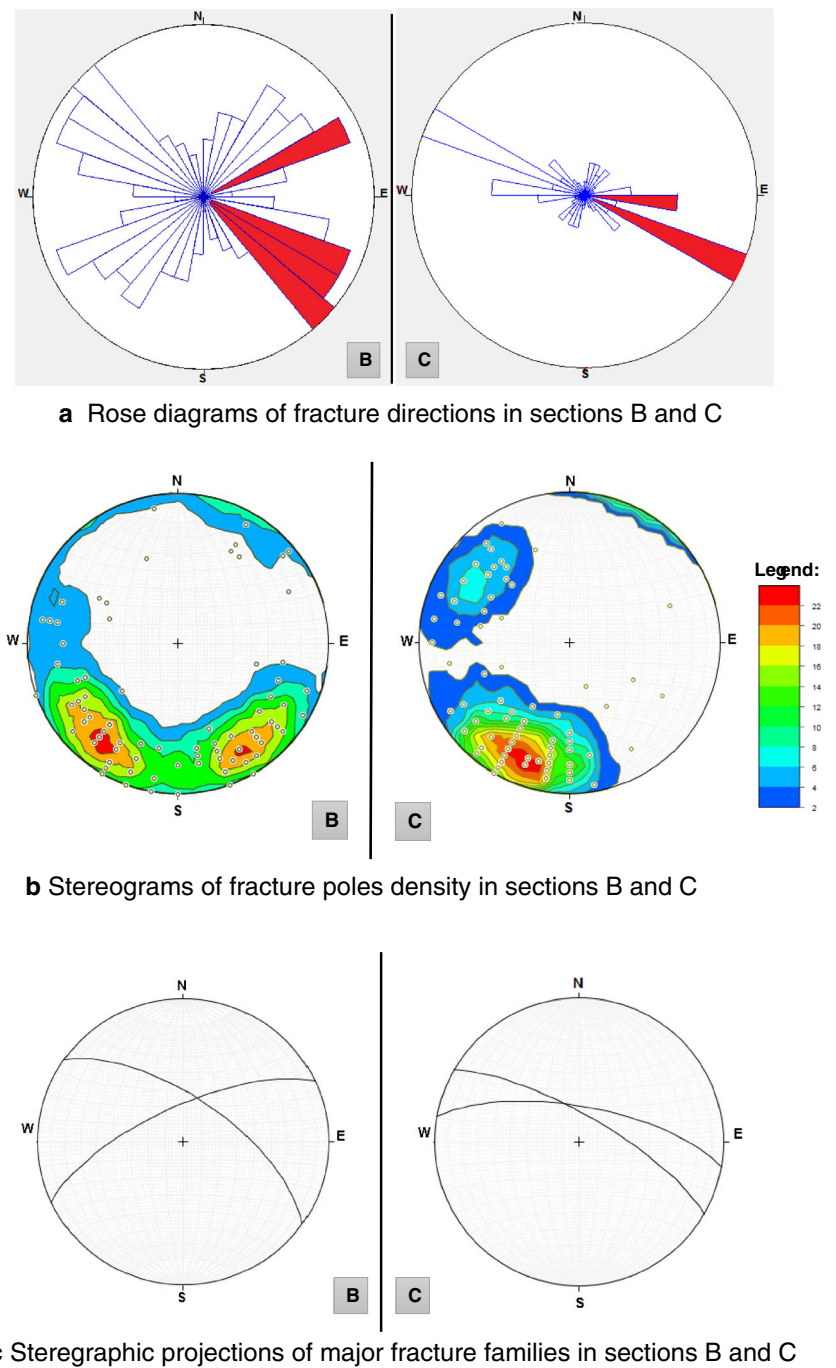


Table 3 Geometric parameters of the major fracture families in sections B and C

Section	Major fracture families	DStrike	Dip	Frequency F_r	Density	Average spacing S_r (m)	Extent (m)
Section B	First family	N100 to N 140	65 SW	0.18	0.276	4.46	4.4
	Second family	N60 to N70	75 SE	0.096		8.3	4.78
Section C	First family	N110 to N120	70 S	1.606	2.015	0.62	4.22
	Second family	N90 to N100	75 SW	0.409		2.43	4.04

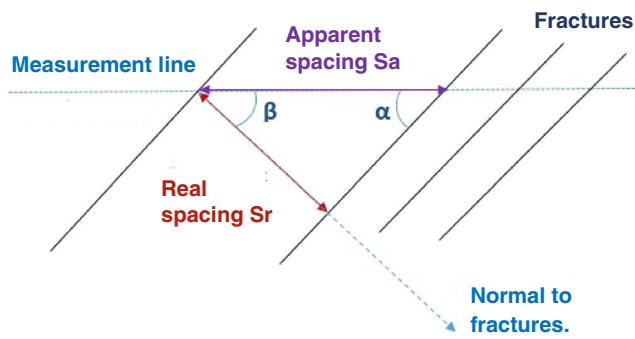


Fig. 11 Schematic representation of the angle between the measurement line and the average orientation of a fracture system

Frequency

The frequency *F* is defined as the number of fractures in each fracture system over a length of 1 m; it can be calculated by dividing the number of fractures of the same family *N* that intersect a measurement line perpendicular to the plane of these fractures by the length of the measurement line *L*:

$$F = N/L$$

Average spacing

The average spacing *S* represents the average distance between the fractures in the same family along the measurement line. It can also be obtained from the calculated frequency, which is equal to its inverse:

$$S = 1/F$$

The distances between fractures are measured along a measurement line. Because the measurement line is generally not perpendicular to the average orientation of the fracture family,

the distances must be multiplied by the sine of the angle between the measurement line and the average fracture orientation. The fracture frequency determined in the field must be divided by the sine of this angle.

The measurement line is along an outcrop, so only fractures that actually intersect the line and not those that are visible on the outcrop but do not reach it should be considered (Fig. 11).

Based on these measurements, we obtain the density and the average spacing of the major fracture families represented in Table 3.

Fracture extent

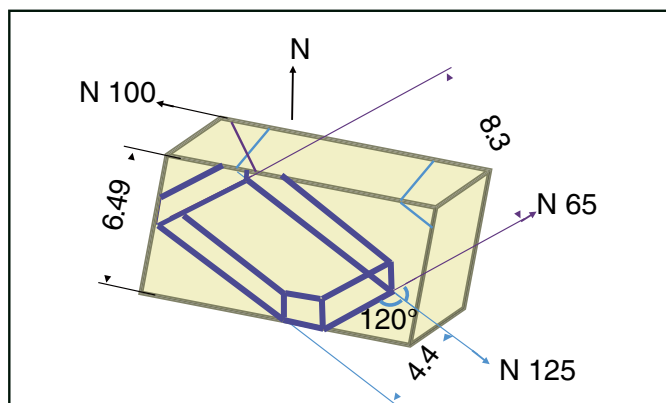
In both sections B and C, all of the fractures are visible in the outcrop; the average extent is directly determined for each major fracture family (Table 3).

Unit block modeling

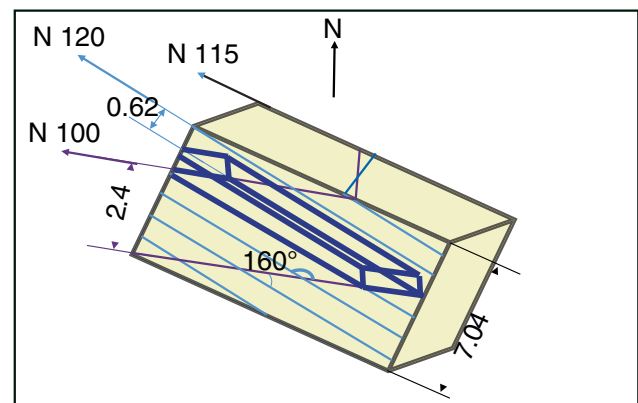
These essential parameters can provide an indication of the average amount of fracturing of the rock mass, which can be used to model a unit block in each section (Fig. 12).

Geomechanical properties

The geomechanical properties of the rocks were determined in the laboratory. The appropriate tests were selected based on the nature of the materials. Shear tests using a Casagrande box were performed on the soil samples (marl and phosphate), and simple compressive strength tests and Brazilian tests were performed on cylindrical rock samples (carbonate, limestone, and gypsum). The results are shown in Table 4.



A unit bloc of dimension (4.74 m; 8.83 m) in section B



A unit bloc of dimension (1.83 m; 7.10 m) in section C

Fig. 12 Three-dimensional modeling of the distributions of major fracture orientations in the carbonate layer in sections B and C

Table 4 Geometric parameters of different materials in the open pit mine area

Materials	Geometric parameters		
	Cohesion (MPa)	Friction angle (degrees)	Specific weight (kN/m ³)
Marl	0.044	15	17.15
Phosphate	0.070	19	20.36
Gypsum	5.614	20	20.36
Limestone	0.048*	40	21.96
Carbonate rock	1.737	30	17.27

Ultimate slope design and stability analysis

The design of the ultimate slope is based on a stability analysis. This study identified the possible failure modes (planar, wedge, toppling, circular) using a kinematic approach (Hoek and Bray 1981; Hoek and Brawn 1988), and the safety factor was calculated using the stability calculation software “SLIDE” based on the limit equilibrium method.

The design process is a trade-off between stability and economics; steep cuts are usually less expensive to construct than flat cuts (Bye and Bell 2001). The design must accommodate the geological conditions within the area of the pit, which may require different slope designs around the pit (Read and Stacey 2009).

The potential failure modes that may occur on either the bench scale or on the scale of the overall pit slope are distinguished based on the characteristics of the materials forming

the slope. Phosphate ore mining requires the excavation of the materials above the ore, which will create two slopes facing each other. One, which faces to the west, exposes a rock mass (carbonate rock, limestone, dolomite); however, the other, which faces east, is composed of marls.

Only one failure mechanism can occur in the marl slope, circular failure, due to this slope’s geometric parameters (e.g., bench height, bench slope angle, berm width, overall slope height) (Fleurisson 2012; Jhanwar and Barsagade 2010; Grenon and Hdjgeorgiou 2010). To prevent the occurrence of this type of a failure, this slope is designed based on the calculated long-term safety factor, which must be greater than 1.4 (Masoud et al. 2016) (Fig. 13).

The designed ultimate slope to be excavated in the marls provides a safety factor of 1.48. Its basic geometric parameters are as follows:

- The angle of the final slopes of the face of the benches is 65°.
- The height of the mine benches is 5 m.
- The width of the berms is 10 m.
- The overall slope height is 42 m.

The slope that will be excavated in the rock mass is composed of three types of materials: a limestone layer, a fractured carbonate deposit, and a gypsum unit. The main failure risk is in the carbonate layer. The stereographic projection of the two major fracture families identified in the fracture study in sections B and C shows the potential for two failure modes: planar failure and wedge failure.

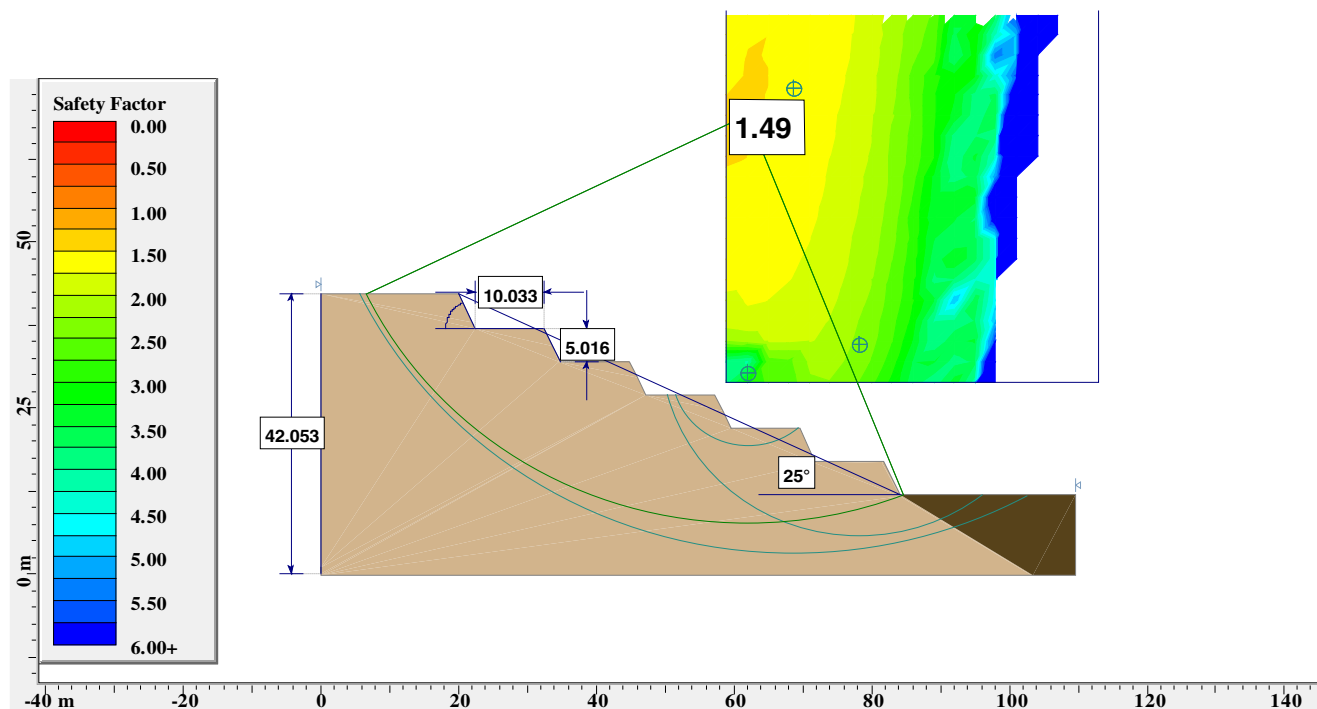
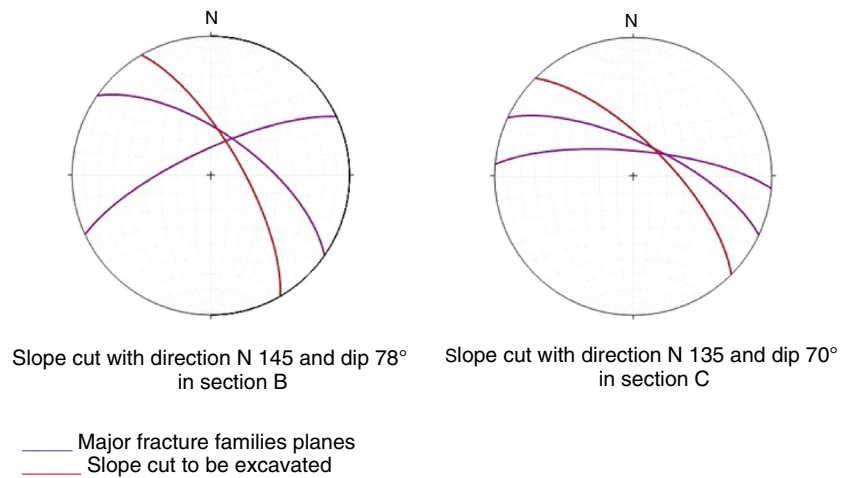


Fig. 13 Stability calculation of the designed slope in marls using the SLIDE software

Fig. 14 Stereographic projections of the slope cut and the major fracture planes (sections B and C)



In the design of cut slopes, there is little flexibility to adjust the orientation of the slope to accommodate the geological conditions, especially the fracture network identified using the kinematic method. The slope face must be more than 20° beyond the angle of the critical fracture to prevent planar failure (ZainAlabideen and Helal 2016).

The kinematic analysis is used to determine not only the appropriate slope orientation to prevent planar failures but also the maximum safe cut angle that will prevent wedge displacements (Um et al. 1996).

In the stereographic projection, sliding along a line of intersection occurs when two discontinuity planes intersect to form a wedge. The maximum safe slope angle is obtained by

the dip of the great circle that passes through the intersection of the two fracture planes (Um et al. 1996) (Fig. 14).

In section B, the failure mode (plane or wedge) follows the planes of the two fracture families with median strikes of N125 and N65 and their intersection. As a result, a slope cut with a strike of N145 (southeast to northwest) and a steep slope (maximum safe slope angle) of 78° towards the SW is used to prevent planar failures on the two fracture families.

In section C, the planar failures follow the two fracture planes, which have median strikes of N115 and N95. Therefore, we use a slope cut with a strike of N135 and a maximum safe slope angle of 70° towards the SW.

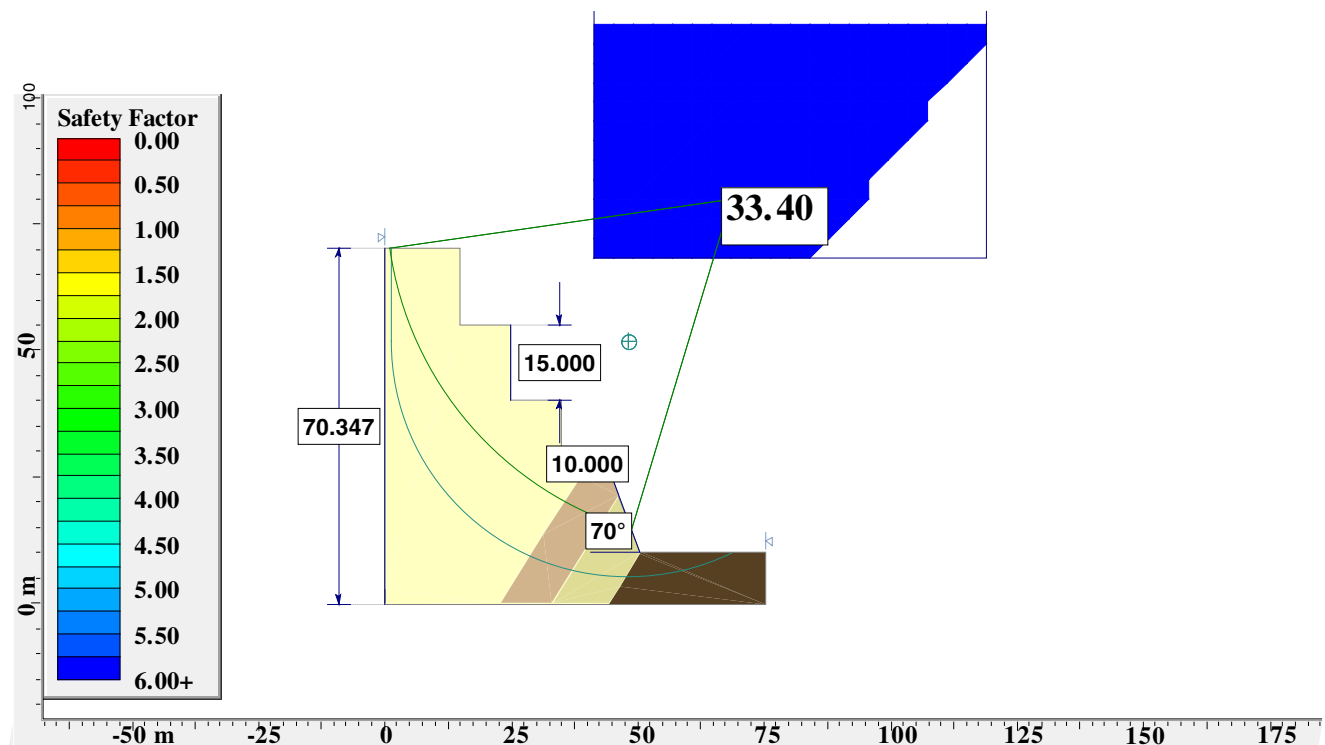


Fig. 15 Stability calculation of the designed slope in the rock mass using the SLIDE software (total height of the ultimate slope = 70 m, bench height = 15 m, berm width = 10 m)

In conclusion, we obtain two similar strikes and two different dips for the slope cuts in the two sections. Therefore, to use a single dip value, we consider the lowest one (70°) as the slope cut angle in both sections. However, this slope cut angle is only applied in the carbonate layer. Because the gypsum unit has no fractures, a vertical slope can be excavated in it. The stability analysis of the final slope design in the rock mass using the limit equilibrium method (SLIDE) indicates that the slope has a safety factor of 33 (Fig. 15).

Conclusion

The preliminary studies presented in this paper are crucial to determining the geological and geomechanical characteristics of the open pit mine area and particularly in the phosphate deposit. The data collected from field observations and laboratory tests represent the basic parameters that are used in the ultimate slope design and stability analysis. The excavation will create two types of slopes around the pit that require different designs. For each slope cut, the geometric parameters are identified using the kinematic and limit equilibrium methods to optimize the slope design that guarantees both stability and favorable economics.

The calculated safety factor ($FS = 1.48$) for the slope designed in the marl is underestimated because of the difficulty of extracting intact samples, which causes a decrease in the cohesion value compared with the real value. In contrast, the stability analysis of the rock slope indicates a very high safety factor ($FS = 33$), which is overestimated because it does not take into account the fractures that can form during mining operations.

The slope designs obtained in this preliminary stage can be updated and modified based on the variations in the geological and geotechnical parameters that are identified throughout the mining operations.

References

- Beji-Sassi A (1985) Petrographie, mineralogie et géochimie des sédiments phosphates de la bordure orientale de l'île de Kasserine (Tunisie). Thèse de doctorat, Faculté de Sciences de Tunis, p150–152
- Bye AR, Bell FG (2001) Stability assessment and slope design at sandsloot open pit, South Africa. *Int J Rock Mech Min Sci* 38: 449–466
- Carreon-Freyre D, Cojean R, Rocchini JF (1996) Geometrical characterization of the fractures network in ornamental rock quarries. Application to the improvement of the Exploitation. *Bull Int Assoc Eng Geol Paris* 54:22
- Chalhoub M (2006) Apports des méthodes d'homogénéisation numériques à la classification des massifs rocheux fracturés. Thèse 3ème cycle, Ecole Nationale Supérieure des Mines de Paris, p 206
- Cojean R, Fleurisson JA (2005) Ciel Ouvert mines et carrières, Élaboration de projets. Approche géologique, hydrogéologique et géomécanique: Géomécanique Appliquée au Ciel Ouvert. *Tech Indus Miner* 26:49–16
- Fleurisson J-A (2012) Slope design and implementation in open pit mines: geological and geomechanical approach. First International Symposium on Innovation and Technology in the Phosphate Industry SYMPHOS 2011. Elsevier Ltd.
- Grenon M, Hadjigeorgiou J (2010) Integrated structural stability analysis for preliminary open pit design. *Int J Rock Mech Min Sci* 47:450–460
- Haji T, Zouaghi T, Boukadi N (2014) The role of inherited structures in the evolution of the Mknassy Basin, Central Tunisia, based on geological-geophysical transects. *J Afr Earth Sci* 96:51–59
- Hoek E, Bray J (1981) Rock slope engineering. Institute of Mining and Metallurgy, London
- Hoek E, Brown ET (1988) The Hoek–Brown failure criterion—a 1988 update. In: *Proc. of 15th Canadian. Rock Mech. Sym., University of Toronto*, pp.31–38
- Jaouadi M (1996) Etude géologique du secteur Jebbes el Meheri (« Axe » Nord-Sud). Apport de la géophysique et de la géochimie à l'étude de la carrière de Kef Abdallah. *Mem. DEA, Univ. de Tunis*, 89 p
- Jaouadi M (2004) Les événements tectoniques du Crétacé supérieur dans le secteur méridional de l'axe Nord-Sud (Tunisie). Thèse 3ème cycle, Univ de Tunis, 183 p
- Jhanwar JC, Barsagade DS (2010) Design of ultimate pit slopes for open cast limestone mines working under the construction of surface structure—a case study. *Min Eng Jr* 11:19–27
- Khessibi M (1978) Etude géologique du secteur Maknassy-Mezzouna et de Djebel Kebar. Thèse 3ème Cycle, Lyon, 175p
- Lafi A, Felhi M, Jaballi F, Guermit F, Trabelsi H, Zayani K, Tlili A (2016) Exploration et cartographie géologique des séries phosphatées du Jebel Jebes (Région de Maknassy, Tunisie Centrale). *Ann Min Geol* 47:200–211
- Masoud SS, Parviz M, Ebrahim Y (2016) Optimizing and slope determination of final wall for Maiduk Mine with consideration of destabilizer factors. In: *Int J Min Sci Technol*, vol 26, pp 501–509
- Porokhovoï E (1995) Stabilité à long terme des talus de mines à ciel ouvert dans les massifs de roches basiques et ultrabasiqes. Thèse 3ème cycle, École Nationale des Ponts et Chaussées, 20–24p
- Read J, Stacey P (2009) Guidelines for open pit slope design, First edn. CSIRO Publishing, Collingwood, p 512
- Ruhland M, Grolier J, Vialon P (1990) Elements de tectonique analytique. Masson, Ed., France 118p
- Singh et al (1994) Slope design of an open pit copper mine. *Int J Rock Mech Min Sci Geomech Abstr* 31(1):55–69
- Tahiri A (1992) Modelisation des massifs rocheux fissurés par la méthode des éléments distincts. Thèse 3ème cycle, École Nationale des Ponts et Chaussées, p222
- Um J-G, Kulatilake PHSW, Chen JP, Teng JR (1996) Maximum safe slope angles for proposed shiplocks of the three gorges dam site based on kinematic analyses performed on major discontinuities. *Proceedings America Society of Mining and Reclamation* pp 267–281
- ZainAlabideen K, Helal M (2016) Determination of the safe orientation and dip of a rock slope in an open pit mine in Syria using kinematic analysis. *Al-Nahrain Univ Coll Eng J (NUCEJ)* 91(1):33–45